Design methodology of a meta-cushion for reducing underwater noise during offshore pile hammering

Azevedo Vasconcelos, Ana Carolina; Van Zijl, Christof; Schott, Dingena; Jovanova, Jovana

DOI
10.1016/j.oceaneng.2025.122197

Publication date
2025

Document Version
Final published version

Published in
Ocean Engineering

Citation (APA)
Azevedo Vasconcelos, A. C., Van Zijl, C., Schott, D., & Jovanova, J. (2025). Design methodology of a meta-cushion for reducing underwater noise during offshore pile hammering. *Ocean Engineering*, *340*, Article 122197. https://doi.org/10.1016/j.oceaneng.2025.122197

Ocean Engineering 340 (2025) 122197

Contents lists available at ScienceDirect

Ocean Engineering

journal homepage: www.elsevier.com/locate/oceaneng

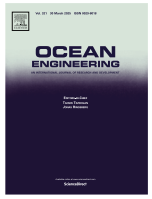

Research paper

Design methodology of a meta-cushion for reducing underwater noise during offshore pile hammering

Ana Carolina Azevedo Vasconcelos*, Christof Van Zijl, Dingena Schott, Jovana Jovanova

Faculty of Mechanical Engineering, Delft University of Technology, Mekelweg 2, 2628 CD Delft, The Netherlands

ARTICLE INFO

Keywords:
Resonant metamaterials
Vibration filtering
Underwater noise
Pile installation

ABSTRACT

The growth of offshore wind farms is accelerating to meet the renewable energy target by 2030, driving the development of larger offshore wind turbines (OWTs) to boost energy capacity. To support these OWTs, large monopiles are being installed by using impact hammers, which in turn emit low-frequency underwater noise, posing challenges for traditional noise mitigation systems and increasing risks to marine life. To address this, a metamaterial-based cushion (meta-cushion) was proposed, embedding resonators to filter longitudinal waves associated with high underwater noise levels. While prior work has demonstrated the meta-cushion's noise attenuation potential, design guidelines are required for adaptation to various monopile installations. This paper introduces, for the first time, a design methodology for the meta-cushion, which based on the input parameters of the monopile system, it details the procedure for selecting the resonant elements contributing to the attenuation performance and their spatial arrangement on the cushion for enhancing mechanical performance. Such performance indicators are evaluated via finite element simulations and experimental modal analyses. The methodology concludes with a nondimensional study of the spiral resonator, which showed the best attenuation response in experiments, exploring its behavior under varying material and geometric parameters. This methodology enables the development of meta-cushions adaptable to monopile installations under any environmental conditions.

1. Introduction

With only half of the planned energy capacity currently installed in Europe, a rapid expansion of offshore wind turbines (OWTs) is expected to meet 2030 targets. Newer OWTs are larger and more efficient (Wind Europe, 2022), and are typically supported by monopile foundations, which offer a cost-effective manufacturing and installation solution. These monopiles, made from steel pipes ranging from 25 to 40 m in length and 4 to 8 m in diameter (Murphy et al., 2018; Wang et al., 2020; Ma and Yang, 2023), are expected to increase in size to support next generation of OWTs. Monopile installation involves driving the pile into the seabed with an impact hammer, which generates longitudinal waves that propagate along the pile, converting to radial motion due to Poisson's effect (Reinhall and Dahl, 2011). This pile motion produces underwater sound waves capable of traveling over kilometers and reaching intensities high enough to harm marine life, potentially causing hearing loss and even death (Kastelein et al., 2015; Solé et al., 2017).

To protect marine life during monopile installation, several noise mitigation systems (NMSs) have been developed, such as noise mitigation screens (Lee et al., 2012), bubble curtains (Bohne et al., 2019), and hydro damping screens (Bruns et al., 2014). The working principle of such systems relies on the impedance mismatch principle—either between water and screen material or between water and bubbles (free or encapsulated)—and resonance phenomenon—free or encapsulated bubbles are designed to resonate at specific frequencies—so that sound waves are reflected or absorbed by the NMS, reducing the sound wave transmission. Effective NMS design requires targeting the frequency ranges of peak noise emissions higher than threshold noise values (Andersson et al., 2017). Tsouvalas (2020) stated that the frequencies of propagating waves are related to the geometric and material parameters of the monopile. His studies indicated that underwater pressure levels are dependent on the ring frequency of the cylindrical shell (f_r) and concentrate at frequencies between $0.5f_r \leq f \leq 0.8f_r$. For a 4 m diameter monopile, this translates to noise radiating between 200 and 350 Hz. The traditional NMSs are effective at frequency ranges around 1000 Hz, where a sound level reduction of 15 dB has been obtained at a distance of 750 m from the pile. However, their efficiency decreases for lower frequencies (Bellmann, 2014), where level reductions below

* Corresponding author.
E-mail address: a.c.azevedovasconcelos@tudelft.nl (A.C. Azevedo Vasconcelos).

https://doi.org/10.1016/j.oceaneng.2025.122197
Received 21 March 2025; Received in revised form 27 June 2025; Accepted 12 July 2025
Available online 25 July 2025

10 dB are observed. Considering bubbly NMSs, which are widely employed during monopile installation, bubbles from 8 mm to 50 mm of radius are required to attenuate low-frequency sound waves. The generation of such bubble sizes is extremely complex, mostly when released from harsh environment, such as turbulent waters, where most of the bubbles will split into smaller parts. As future monopiles increase in size (von Pein et al., 2022), addressing these lower frequencies will demand innovative solutions.

As a new solution to reduce the low-frequency underwater noise, we proposed in our previous work (Vasconcelos et al., 2024) a redesigned based on locally resonant metamaterials (Hussein et al., 2014). This metamaterial-based cushion, or meta-cushion, is placed between the impact hammer and the monopile, filtering out longitudinal waves tied to the monopile's radial resonance through its resonant internal elements distributed in longitudinal arrays. This reduces underwater sound wave propagation, protecting marine life while allowing essential installation vibrations to pass through. The principle of the meta-cushion was verified in a pile-water-soil interaction model using finite element simulations, which showed noise reduction at resonance-related frequencies. To target even lower frequencies, the meta-cushion employs spiral-shaped unit cells with curved beams for reduced stiffness, which have been demonstrated improved attenuation performance. A follow-up study proposed in our group experimentally validated this filtering effect, exploring combinations of multiple resonator designs to broaden the attenuation range across varied frequencies. With the meta-cushion principle verified and validated, a framework can now be established to guide designers in systematically selecting resonator types and array distributions for a meta-cushion tailored to any monopile hammering procedure.

This paper aims to propose a novel design methodology for a meta-cushion that reduces underwater noise from offshore monopile hammering. The methodology is divided into four blocks, as shown in Fig. 1, consisting of the identification of input parameters, the evaluation of performance through numerical studies, the experimental validation of prototype designs, and full-scale design analysis. In the first block, key input parameters for critical noise levels are identified and applied to the design of the meta-cushion's resonant elements. These elements are assembled in various configurations, from which structural features critical for high-impact loads are evaluated. In the second block, numerical models are developed to examine the attenuation principle and mechanical features of potential meta-cushion designs, along with underwater noise measurements. This potential designs are then manufactured and experimentally tested in a small-scale monopile setup, consisting the third block of the design methodology. The resonators exhibiting the best attenuation properties and configurations with highest mechanical performance are selected for performing a nondimensional analysis in the final block, where their potential for noise attenuation across multiple frequency ranges and multiple scales by adjusting unit cell size and material properties. This design methodology provides a systematic approach to developing meta-cushions with potential to reduce underwater noise during monopile installation under any environmental conditions.

2. Design methodology for a meta-cushion

This section introduces the design methodology employed for developing a meta-cushion for reducing noise levels during pile hammering process, from which input parameters are defined and the procedure for selecting and investigating the noise attenuation and structural performance is presented. A schematic of the proposed methodology is illustrated in Fig. 1.

In the initial block, monopile dimensions, impact hammer energy, and the seawater depth (Deng et al., 2016; von Pein et al., 2022) are extracted from a full-scale monopile installation. Given the high costs of full-scale experimental evaluations, a scaled-down model with adjusted input parameters is defined using appropriate scaling laws. These updated parameters establish the critical noise levels, which are then used to design resonators capable of reducing noise below the threshold.

After selecting the designs, the resonator are arranged in arrays that will be assembled to constitute several meta-cushion configurations. Numerical studies will assess the noise attenuation performance, focusing on attenuation range and amount of resonators. Then, structural

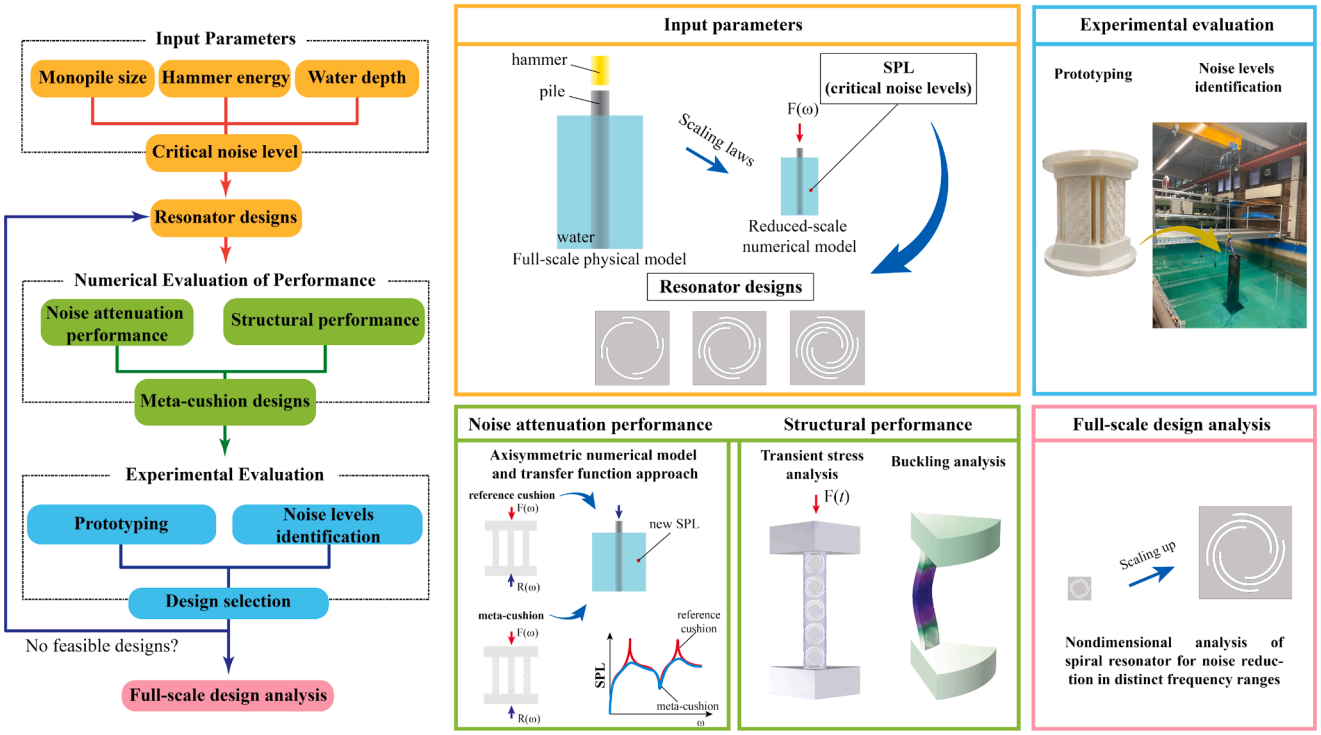

Fig. 1. Schematic of design methodology for a meta-cushion for reducing underwater noise during monopile driving process.

analysis is performed to evaluate transient stresses and critical buckling loads that will give the most suitable array distribution for the applied hammer energy. From such studies, final meta-cushion designs are selected.

In the third block, meta-cushion prototypes are fabricated and tested in a small-scale setup to evaluate noise attenuation performance. If the resonator designs demonstrate sufficient performance, they can advance to further investigations for potential full-scale monopile applications, constituting the final block of the design methodology. Otherwise, new resonator designs will be explored and tested again. The following sections discuss each design step through a scaled-down case study.

3. Input parameters

Designing the meta-cushion begins by identifying the frequencies associated with high noise levels, which depend on monopile dimensions, water depth, and impact hammer characteristics (energy and frequency spectrum content), as well as soil properties. Since full-scale offshore impact tests are extremely expensive, case studies are often scaled down for performing the vibro-acoustic analysis. Due to limited access to hammer and soil data, this work demosntrates how to determine impact load when scaled hammer energy is known. Then, the scaling laws related to the monopile are introduced.

The strike hammer energy E is numerically modeled as the vertical pile head velocity profile $v(t)$, which is given by Deeks and Randolph (1993)

$$v(t) = v_0 \exp\left(-Z/m_r t\right), \tag{1}$$

where v_0 is the initial velocity of the ram, derived from the strike energy and expressed as $v_0 = \sqrt{2E/m_r}$, m_r is the ram weight, and Z is the pile head impedance, expressed as $Z = E_p A_p / c_p$, being E_p, A_p, and c_p the Young's modulus, cross sectional are of the pile head, and the longitudinal wave speed of the pile, respectively.

As a start point of this work, a monopile is designed through scaling laws to keep the dimensions consistent with full-scale monopiles. Typical offshore monopiles are made of steel and have embedded length L (below sea surface level) of 25–40 m and diameter D of 4–8 m, which correspond to an aspect ratio (L/D) in the range of 3–8 (Murphy et al., 2018; Wang et al., 2020; Ma and Yang, 2023). For the description of the proposed design approach, an aspect ratio of 7.3 was chosen for the testing monopile, which has been defined according to water depth of the testing tank available for the experimental evaluation stage. Further information about the scaled monopile is given in Table 1.

Once defined the monopile dimensions, a vibro-acoustic numerical model is developed to predict the potential noise frequency ranges. To that end, an axisymmetric numerical model containing a pile partially submerged is proposed, as shown in Fig. 2a. The monopile is assumed as a shell structure and water is represented by an acoustic medium. To reduce the effects of wave reflections, perfectly matched layers (PMLs) are included and zero pressure is assumed at the water surface. Since the focus of this work is investigate the main noise propagation path, from pile direct to water, soil effect is neglected and replaced by a rigid boundary although soil contributions can be easily incorporated as shown in our previous work (Vasconcelos et al., 2024). A zero displacement condition is applied at the bottom edge of the pile and acoustic-structure boundary is used to couple the pile vibrations and acoustic emission. To capture the physics of waves propagating at a specific frequency, the maximum element size h is defined as

$$h = \frac{\lambda}{5} = \frac{1}{5}\frac{c}{f_{\max}}, \tag{2}$$

where $\lambda = c/f_{\max}$ is the minimum wavelength determined by the minimum wave speed c in a domain and the maximum frequency $f_{\max}$ where waves of interest propagate, and the number five indicates the amount of finite elements per wavelength.

Due to limited access to full-scale hammer data, the excitation load is assumed as a time-harmonic ring load with a 1 N amplitude, applied to the top shell edge (indicated by red ring in Fig. 2a), with a frequency range of 1 to 1500 Hz, corresponding to the frequency range of the tested hammer, as will be described later—if full-scale impact load data were available, it could be scaled and used in this model. The numerical model's outputs include acceleration on the pile wall measured at $1.5D$ from the top, according to the American Society for Testing and Materials (ASTM) D4945 standard (ASTM, 2008), and sound pressure levels in water at 1 m and 2 m from the pile wall. Fig. 3 shows the radial and axial accelerations at the pile wall and the sound pressure levels on the chosen points. The peaks presented in both response are associated to the natural frequencies of the monopile, which have been extracted from an eigenfrequency analysis of the proposed axisymmetric model and have been indicated by the vertical lines. Based on the proposed model, the highest peak occurs in the third natural frequency of the monopile (546 Hz), which would require a resonator design filtering such range; however, additional designs are proposed to attenuate multiple frequency ranges.

Four spiral resonator designs have been selected, with their geometric parameters and attenuation zones—or band gaps—summarized in Table 2. PLA was chosen as the constituent material due to its availability for fabrication via FDM in the next design stage. The mechanical and material properties of PLA are Young's modulus E = 3.16 GPa, density $\rho = 1250\,\text{kg/m}^3$, and Poisson's ratio $\nu = 0.33$. Because PLA properties have frequency-dependent behavior, viscoelasticity is included in the numerical model by modifying the stress tensor, which is given by

$$\sigma_v = \left(K' + iK''\right)\epsilon_e, \tag{3}$$

where K' is the storage modulus, K'' is the loss modulus, σ_v is the viscoelastic stress tensor, and ϵ_e is the strain tensor of the elastic model. The storage and loss moduli are obtained via dynamic mechanical analysis (DMA), where a force oscillating at a set frequency is applied at PLA samples under varying temperatures (Leng et al., 2011). Extensive literature exists on using DMA to obtain viscoelastic properties of neat and composite polymers (Muthui et al., 2015; Thumsorn et al., 2022; Kontou et al., 2024). For PLA samples manufactured under similar conditions as the ones presented in this work, the storage and loss moduli are, respectively, $K' = 2220$ MPa and $K'' = 112.9$ MPa.

Two designs show band gaps at zones near the natural frequency of the monopile, while designs II and IV present, respectively, high and low frequency attenuation zones. In the next section, the selected resonator designs are assembled into meta-cushion designs, from which their attenuation and mechanical performance are evaluated.

Table 1
Geometric and material parameters of the scaled monopile.

Parameter	Pile	Parameter	Tank
Length L	2.4 m	Water depth	2.2 m
Diameter D	0.3 m	Width	3.4 m
Thickness t	3 mm	Density ρ_w	1000 kg/m^3
Young's modulus E_p	205.8 GPa	Sound speed in water c_w	1500 m/s
Density ρ_p	7850 kg/m^3	–	–
Poisson's ratio ν_p	0.3	–	–

4. Numerical analysis of meta-cushion principle

In this section, the second block of the design methodology is addressed, where numerical analyses of the resonator designs are conducted to evaluate performance based on two metrics. First, the noise attenuation capacity of each resonator design is verified. Then, the resonators are assembled into various meta-cushion configurations with different numbers and types of resonators, from which their attenuation performance is compared to reference cushions without resonators. Second, to ensure that the meta-cushion remains in the elastic regime, transient stress levels and critical buckling loads are evaluated, from which the suitable configurations are selected.

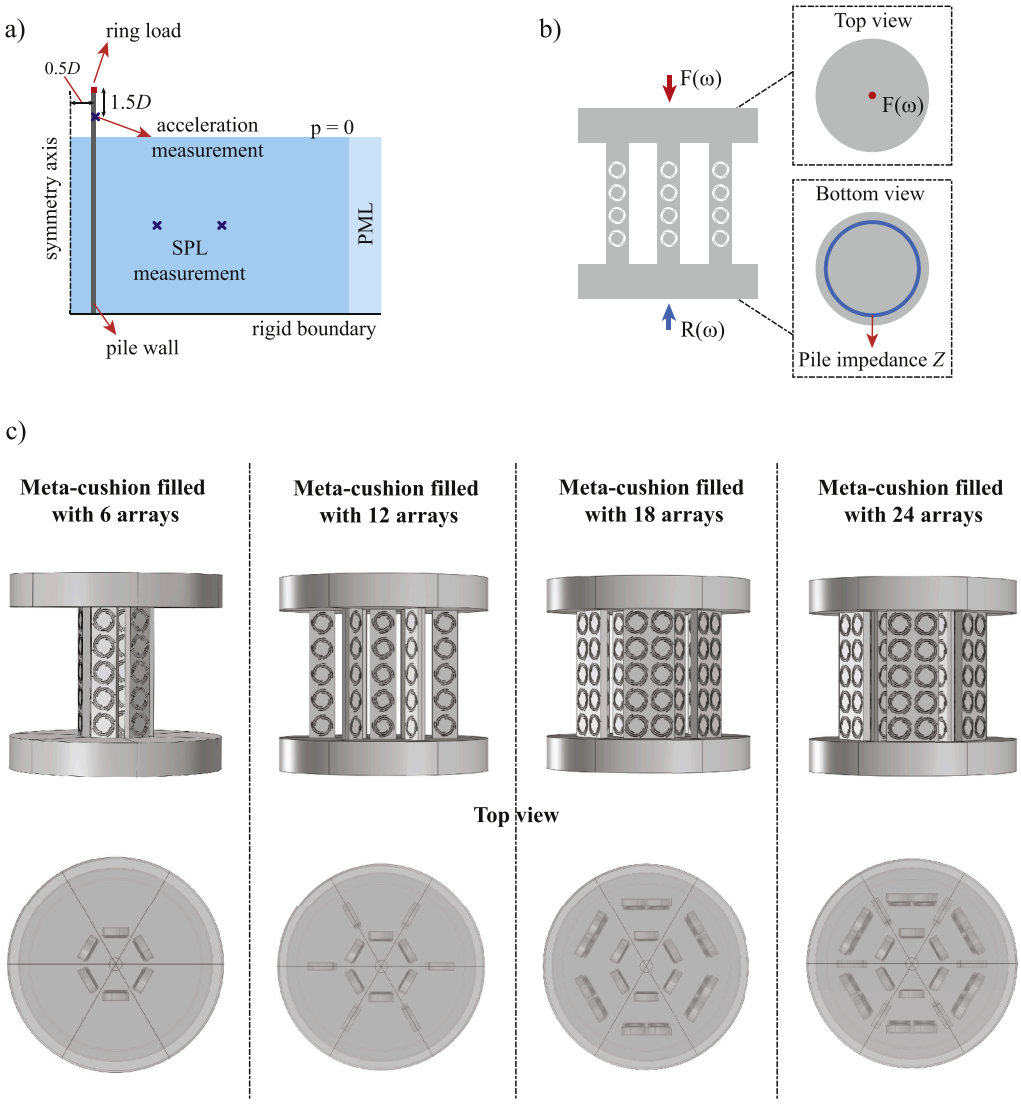

Fig. 2. a) Vibro-acoustic numerical model for calculating the responses in the pile wall and underwater; b) Transfer function approach for calculating the reaction load, used to update the vibro-acoustic model; c) Numerical designs of the meta-cushions containing 6, 12, 18, and 24 arrays.

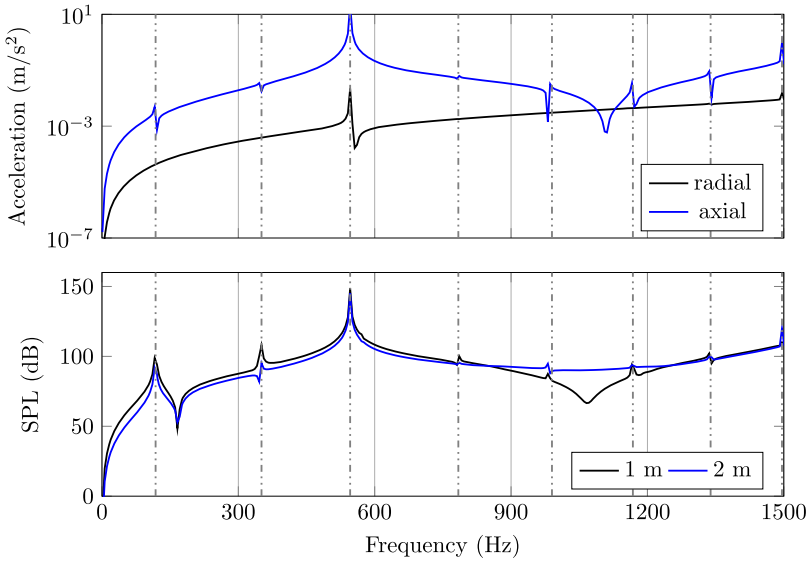

Fig. 3. Acceleration and sound pressure levels measured at the axisymmetric vibro-acoustic model for evaluating potential noise frequency ranges. The vertical lines indicate the natural frequencies of the monopile obtained though the same model.

Table 2
Geometric parameters of selected spiral resonator designs. The last column indicates the attenuation zones identified through a transmission loss analysis.

Spiral design	Geometric parameters			Attenuation zone	
	a [mm]	θ_I [rad]	θ_F [rad]	t_b [mm]	$[f_i, f_f]$ [Hz]
I	40	$\pi/4$	$8\pi/5$	1.2	[580, 605]
II	40	$\pi/2$	$8\pi/5$	1.2	[895, 1070]
III	40	$3\pi/5$	$19\pi/10$	1.2	[475, 525]
IV	40	$\pi/4$	$7\pi/4$	2.0	[265, 285]

Table 3
Meta-cushion configurations for verification of single and multiple attenuation zones. The number six indicates the amount of arrays involved in the assembly.

Array	Meta-cushion configurations								
	A	B	C	D	Comb1	Comb2	Comb3	Comb4	Comb5
I	6	–	–	–	6	–	–	6	6
II	–	6	–	–	6	6	6	6	6
III	–	–	6	–	–	6	–	6	6
IV	–	–	–	6	–	–	6	–	6

For the first design aspect, the resonator designs in Table 2 are arranged into arrays that will form single and combined meta-cushion configurations. The single configurations consist of six arrays in a hexagonal arrangement (see Fig. 2c) and are labeled as configurations A, B, C, and D (Table 3). To enable multiple-frequency filtering, six arrays of different types are combined, which give the remaining configurations listed in Table 3. The arrays of combined cushions are distributed according to the amount of arrays, as shown in Fig. 2c.

Modeling the meta-cushion design directly in the vibro-acoustic model would considerably increase computational costs, so a transfer function approach is used instead. Here, the ring load in the original model is replaced by the meta-cushion contribution expressed as a reaction force (see Fig. 2b). To compute this reaction force, a numerical model of the meta-cushion is developed as shown in Fig. 2c. Symmetry is explored to reduce computational costs, with only one-sixth of the geometry analyzed under cyclic symmetry. The mesh size has been defined according to Eq. (3) to capture wave propagation behavior in the frequency range of interest and mesh refinement has been applied in the resonators' edges and vertices. A 1 N time-harmonic point load is applied to the meta-cushion top plate. The monopile is replaced by a dashpot (total damping constant of 1.1251E5 N.s/m based on the pile head impedance Z) and the reaction load is calculated at the cushion-monopile interface. This reaction load then serves as a ring load in the vibro-acoustic model, where output parameters are measured. Fig. 4 presents radial acceleration and sound pressure level results at 1 m from the pile wall for single cushion designs A, B, C, and D, with arrays containing five, seven, or ten spiral resonators. Gray areas indicate the band gap locations as described in Table 2. The meta-cushion results are compared with reference cushions to assess the resonant effects, revealing reduced monopile acceleration in band gap areas, which also lowers sound pressure levels. This effect enhances by adding more resonators to the meta-cushion, where reductions up to 40 dB in SPL are observed. Among the designs, cushion B gives the broadest band gap, particularly with the maximum number of resonators, while cushion D provides minimum attenuation even when using the maximum amount of resonators.

The same analysis is conducted for the combined meta-cushion configurations, with results shown in Figs. 5 and 6 for arrays containing 10 resonators. The inclusion of different resonator types introduces additional dynamic behaviors (extra peaks) compared to the reference cushion, yet drops in SPL measurements are still observed at the designed band gaps, with resonator type II exhibiting the widest band gap. Notably, some designs exhibit limited attenuation zones due to the boundary conditions applied; when arrays are positioned far from the loading area, generated waves may behave more complexly and not propagate

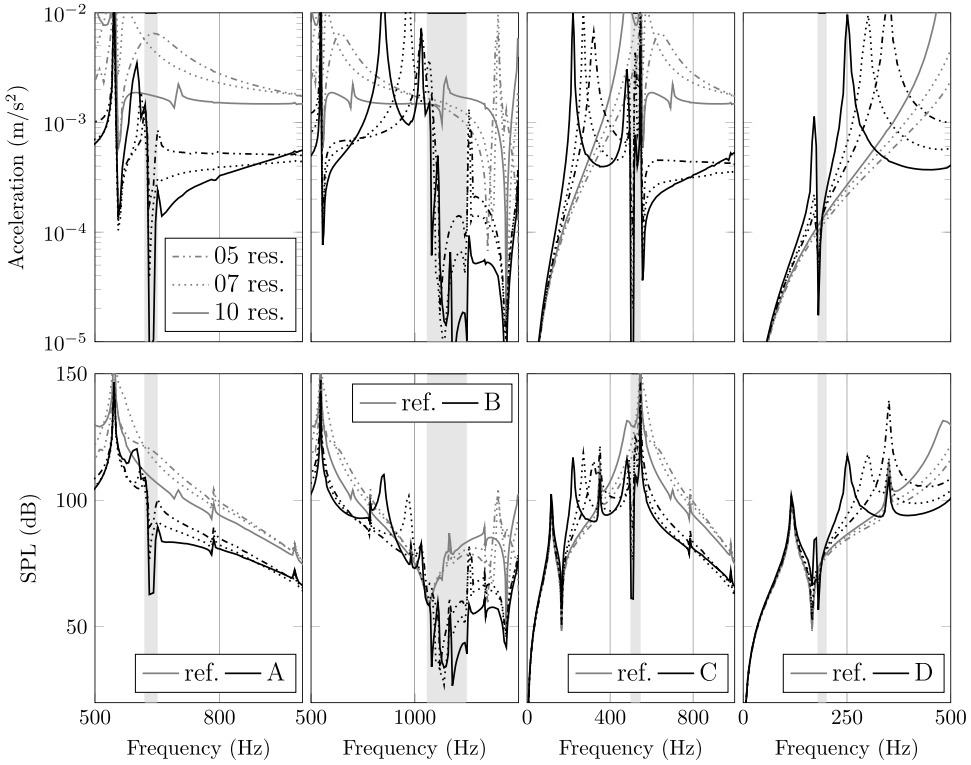

Fig. 4. Acceleration and sound pressure levels measured at the axisymmetric vibro-acoustic model when including the contribution of the single meta-cushion designs with distinct number of resonators (res.) per array. The gray areas indicate the attenuation zones of the designed resonators. The gray and black curves indicate the response for the reference cushion (ref.) and meta-cushion configurations A to D, respectively.

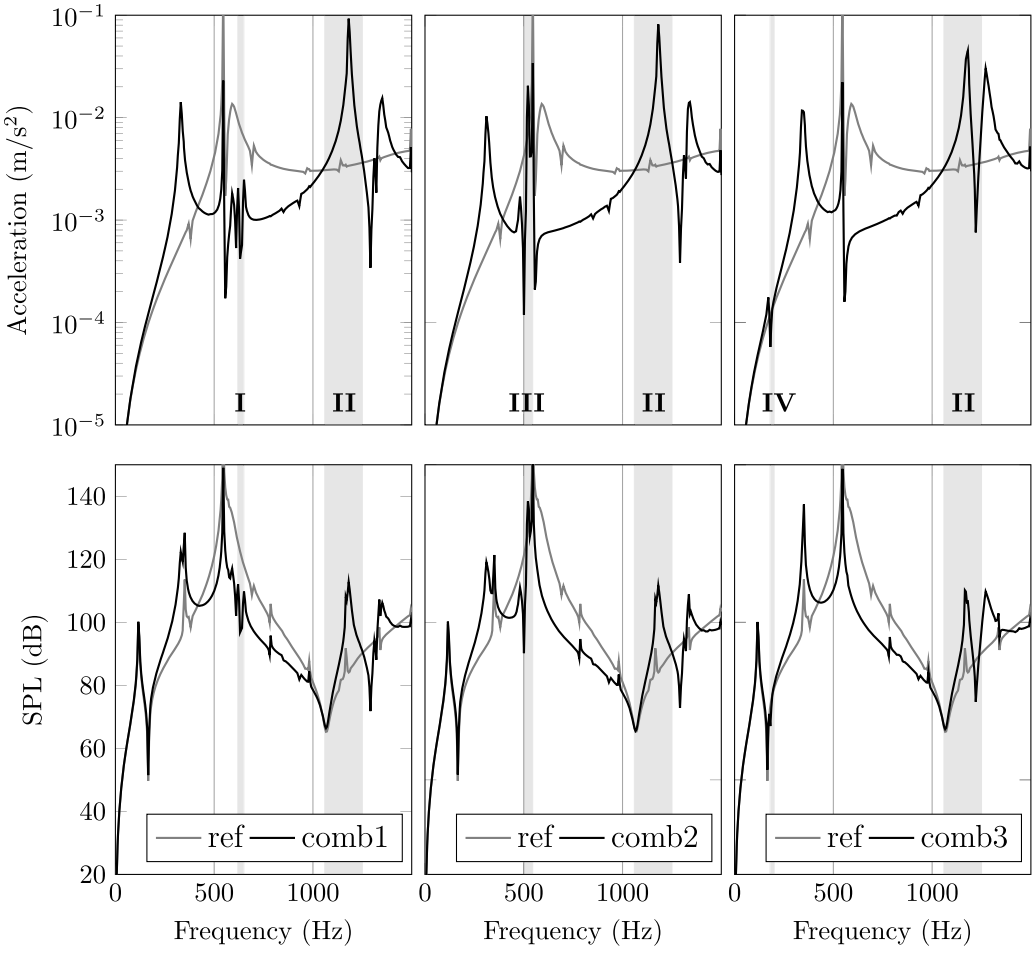

Fig. 5. Acceleration and sound pressure levels measured at the axisymmetric vibro-acoustic model when including the contribution of the reference and combined meta-cushion designs 1 to 3 containing 10 resonators. The gray areas indicate the identified attenuation zones according to the resonator types (I-IV).

purely longitudinally, as assumed for the attenuation zones determination in Table 2. A second reason is the narrow band gap generated–which is the case of meta-cushion containing resonators of type IV, where a slight attenuation is identified in the FRF of combination 3 in Fig. 5 and combination 5 in Fig. 6. Thus, when designing the meta-cushion, arrays that attenuate less critical noise could be placed farther from the impact load—if such load behaves as a point load—or less resonators are incorporated to the arrays when the impact load is applied to the entire top plate.

After determining the meta-cushion's attenuation performance, transient stress levels are evaluated for each configuration subjected to a transient point load given by the pressure expression $P(t) = 20e^{(-t/0.01)}$[kPa], which is a typical expression used to described the load of an impact hammer (Dahl et al., 2015). Note that the stress amplitude is according to the load feature presented in the attenuation performance, however it can be replaced when hammer data is accessible. The monopile is once again replaced by a dashpot, as described in the analysis of the attenuation performance. Fig. 7 displays the time history of maximum Von Mises stress for each configuration and varying array sizes. The maximum Von Mises stress reduces as the number of arrays increases and develops more rapidly for shorter cushions. Snapshots at the peak stress moment, shown in Fig. 8, reveal stress concentrations near the initial points of the curved beams and in the narrow regions between the spiral shapes and the array edge. Further studies are needed to optimize array geometry for better stress distribution under impact loads. The arrangement of spiral arrays through the meta-cushion plates also helps reduce stress concentration, as indicated by the maximum values in Fig. 8.

Since the meta-cushion is a cylindrical structure with relatively thin beams under axial compressive load, the critical buckling loads for each configuration and array size should be evaluated to estimate the meta-cushion's structural integrity under such loading conditions. To that end, a linear eigenvalue buckling analysis is performed, where the same boundary conditions of the transient study have been used, except that the load is replaced by a static unit load used to determine the initial stress states. The eigenvalues, which give the critical loads, are exhibited in Table 4, while the eigenmodes are indicated in Fig. 9. Note that the critical load roughly doubles from 6 to 12 arrays and from 12 to 18 arrays, however, it slightly decreases from 18 to 24 arrays, due to an eigenmode associated to the arrays placed on the middle of the meta-cushion, as exhibited in Fig. 9d. Moreover, increasing the amount of resonators in each array decreases the critical load by almost half. Therefore, if additional resonators are needed to attenuate pile vibration, designs with more arrays are preferable.

5. Experimental evaluation of the meta-cushion designs

In the third block of the meta-cushion design methodology, the meta-cushion designs proposed in the previous section will be experimentally evaluated in terms of their ability in reducing the monopile vibration at specific frequency ranges and consequently reducing the underwater noise. To that end, physical prototypes of the meta-cushion are

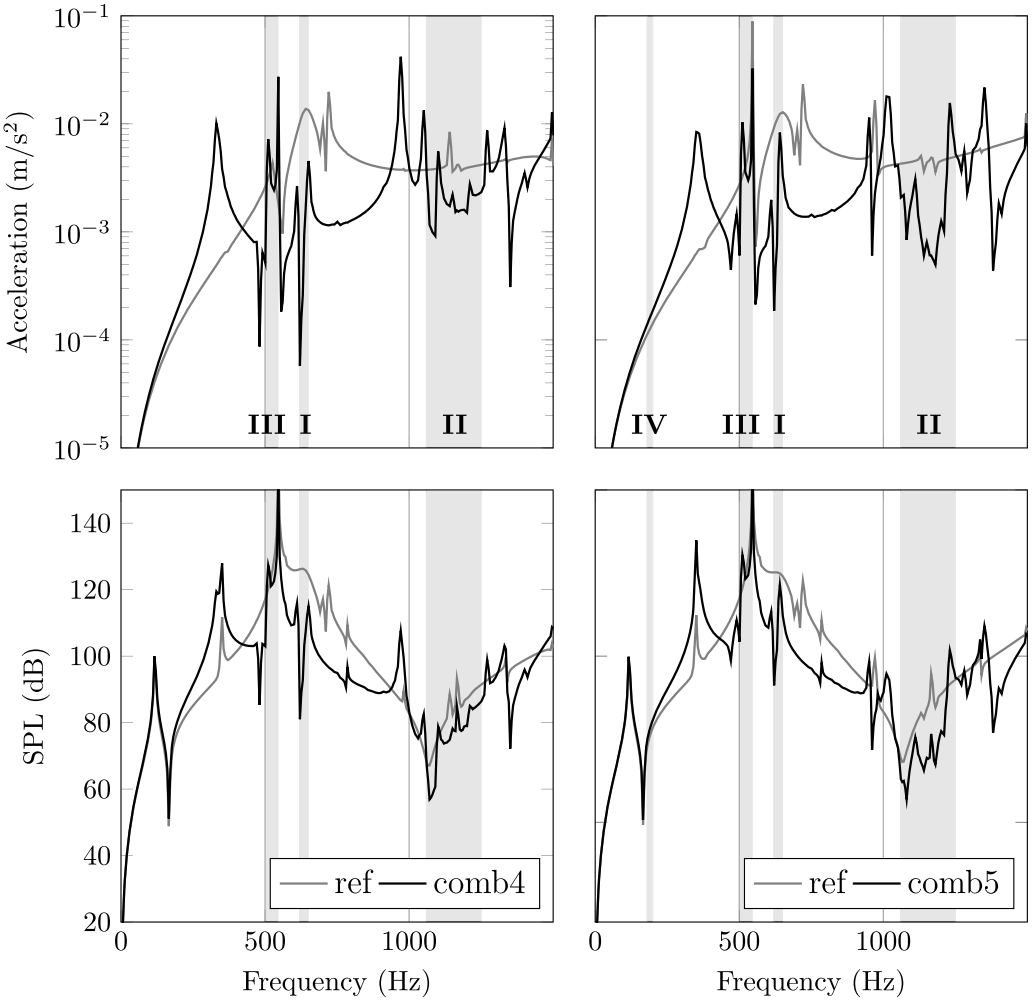

Fig. 6. Acceleration and sound pressure levels measured at the axisymmetric vibro-acoustic model when including the contribution of the reference and combined meta-cushion designs 4 and 5 containing 10 resonators. The gray areas indicate the identified attenuation zones according to the resonator types (I-IV).

developed as displayed in Fig. 10, where they are formed by arrays containing the resonant elements (Fig. 10a) and the plates containing 24 cavities where such arrays are inserted (Fig. 10b). All meta-cushion parts are made of PLA and are manufactured via the 3D printing process FDM, where the arrays contain 100 % infill and the plates contain 15 % infill—the reason for that is to reduce the damping effects of the plates. Because of limitations in the printer bed size, the arrays contain only five resonators.

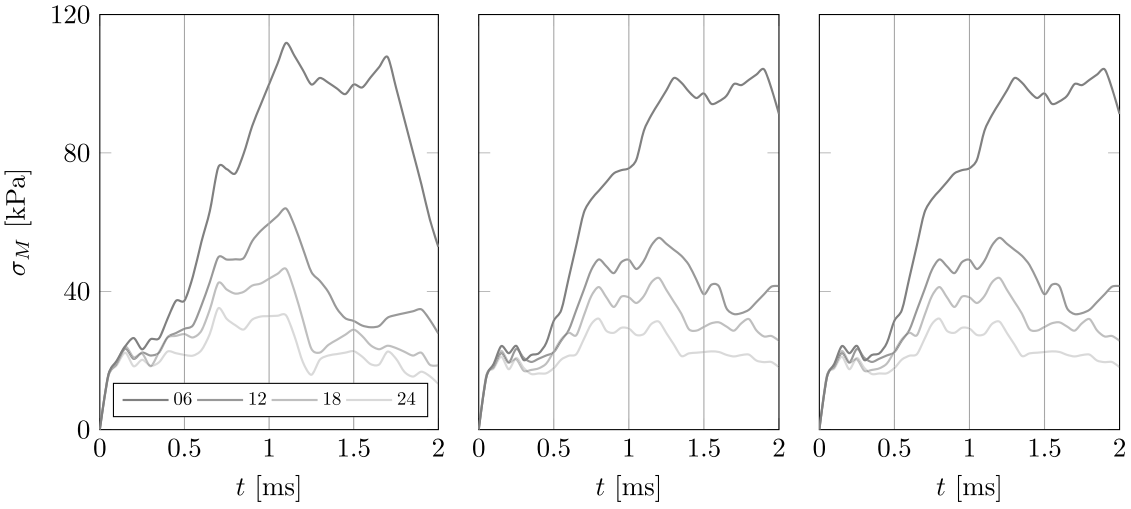

Fig. 7. Time history of maximum von Mises stress for each configuration of meta-cushion containing 5 (left), 7 (middle), and 10 (right) resonators per array.

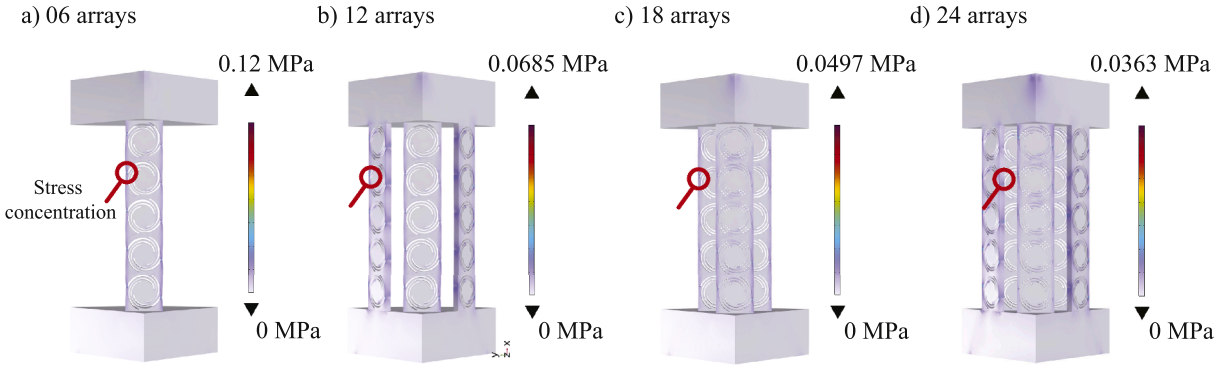

Fig. 8. Snapshot of maximum Von Mises stress field for meta-cushions containing a) 6, b) 12, c) 18, and d) 24 arrays. The colormap indicates the maximum Von Mises value, while the red circles indicate the stress concentration.

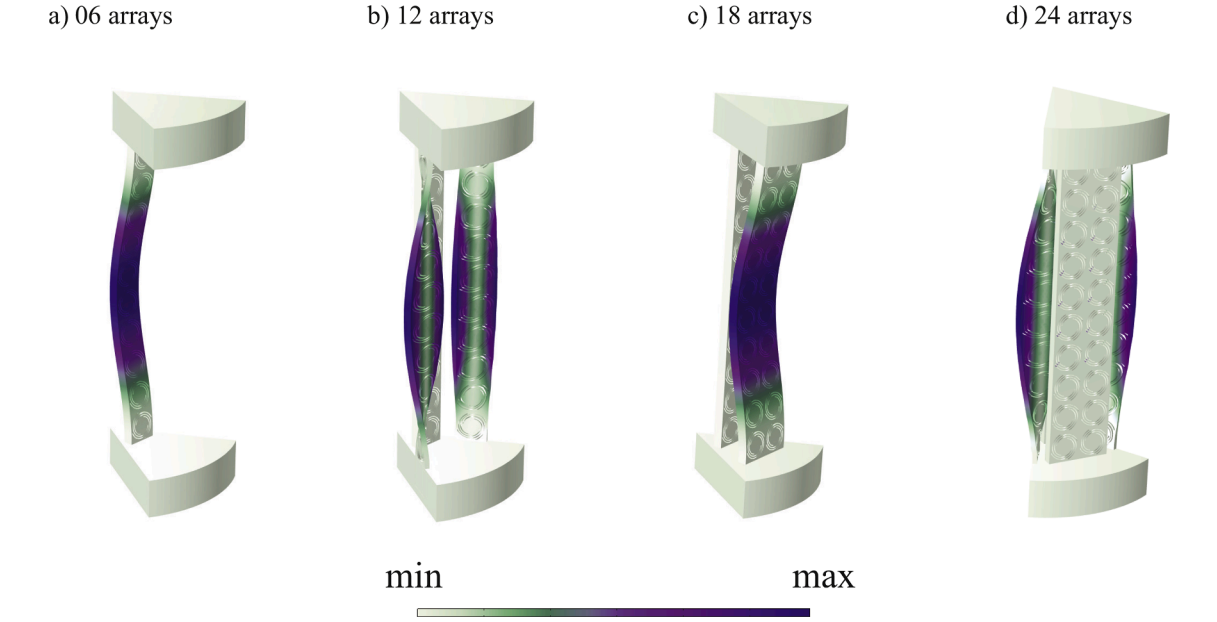

Fig. 9. First buckling mode of meta-cushions containing a) 6, b) 12, c) 18, and d) 24 arrays. The colormap indicates the deformation field.

To verify the presence of band gaps in the physical models, a modal impact analysis testing is initially performed in the printed arrays (Fig. 10a). In this testing, an modal impact hammer delivers an impact load to one end of the arrays and acceleration is measured in the opposite end by using accelerometers. The impact load is generated by a modal impact hammer (Type DJB of model IH/02) containing a force transducer with sensitivity 2.58 mV/N. Similarly to the numerical analysis, the load frequency varies from 1 to 1500 Hz, where the load spectrum energy is concentrated. Transfer functions are obtained through the ratio between the acceleration signal $a(x, y, z, \omega)$ at a point (x, y, z) and the excitation signal, $F(\omega)$, which are given as

$$T_a(x, y, z, \omega) = \frac{a(x, y, z, \omega)}{F(\omega)} \tag{4}$$

Fig. 11 highlights the transfer functions T_a for each designed array obtained by the viscoelastic and experimental analysis. The viscoelastic model agrees well with the experimental measurements. As also indicated by the numerical models, the band gaps of resonator designs I, III, and IV, although located in low-frequency ranges, are narrow, which may not give significant contributions for the noise attenuation. This could be overcome by introducing more resonators in the arrays as observed in Fig. 4.

Table 4
Critical loads in Newton of each meta-cushion configuration with varied array sizes.

Amount of resonators	Amount of arrays			
	6 arrays	12 arrays	18 arrays	24 arrays
5	2988 N	4537 N	9409 N	9271 N
7	1580 N	2246 N	5003 N	4581 N
10	789 N	1053 N	2482 N	2145 N

Once the arrays exhibit the desired attenuation zones, the meta-cushion is assembled according to the configurations defined in Tab 3. To assess the ability of the meta-cushion in reducing the underwater noise, we replicated the hammering of an offshore monopile in the towing tank of the lab facilities in TU Delft. Fig. 12 shows the experimental setup for performing the hammering test. The tank has a water depth of 2.2 m and width of 4.2 m. The monopile was manufactured by folding and welding two steel sheets. Then, the monopile is placed inside the tank with the aid of a crane. To ensure central placement, a rubber plate was used to adjust its position. This bottom restriction may slightly deviate from the zero-displacement boundary condition assumed in the numerical model, as the monopile is not rigidly fixed to the tank.

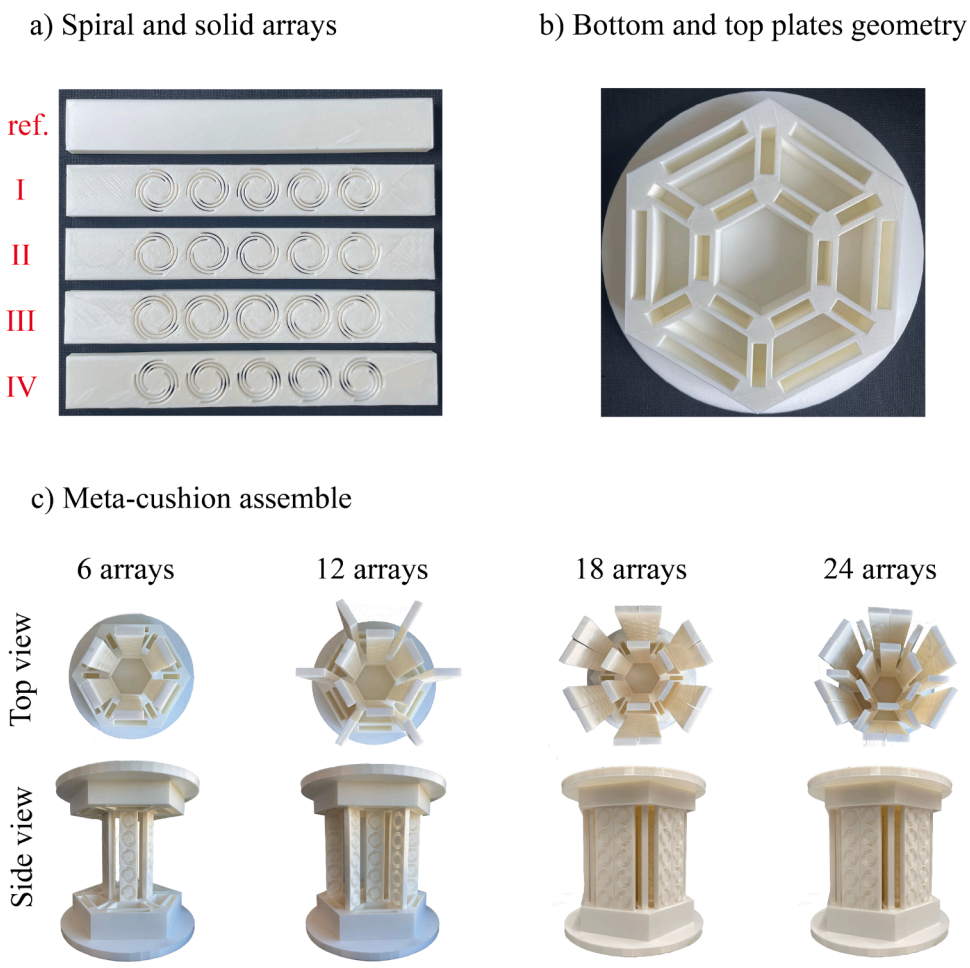

Fig. 10. Printed cushion parts: a) spiral (I, II, III, and IV) and solid (ref.) arrays; b) top and bottom plates. c) Assembled meta-cushion configurations containing 6, 12, 18, and 24 arrays.

Additionally, the response to hammer excitation may differ due to the manufacturing process: unlike the continuum cylindrical pile in the numerical model, the physical model consists of two flat metal sheets folded and welded to form the same cylindrical shape and length. Two hydrophones (Fig. 12b) are placed in the middle of the tank, so that they are aligned with the center of the monopile. The closest hydrophone of model RB9-ETH (6370) is placed 1 m away from the pile wall, while the second hydrophone of model SC2-ETH (6083) is placed 2 m from the pile wall. A pressure sensor was placed at the same height of the hydrophones, but closer to the tank wall (one quarter away from THE tank wall). Transfer functions are obtained through the ratio between the pressure signal $p(x, y, z, \omega)$ at a point (x, y, z) and the excitation signal, $F(\omega)$, which are given as

$$T_p(x, y, z, \omega) = \frac{p(x, y, z, \omega)}{F(\omega)} \tag{5}$$

To express the force to pressure transfer functions in terms of the reference value in water $T_w = 1\mu$ Pa N^{-1}, Eq. (5) is modified by $20\log\left(|T_p|/T_w\right)$.

The impact load is generated by the same modal impact hammer used for obtaining the arrays' transfer functions. To measure the pile acceleration in the radial direction, two accelerometers are installed on the pile wall from a distance of $1.5D$ from the pile top surface, according to the American Society for Testing and Materials (ASTM) D4945 standard (ASTM, 2008). Transfer functions related to the monopile acceleration are also obtained through Eq. (5).

As performed in the numerical evaluation, the monopile vibration is initially investigated to identify the natural frequencies related to the critical noise levels. Fig. 13 shows the frequency response function of the averaged accelerometer data from the monopile wall when the pile is axially hit fifteen times by a modal impact hammer without a cushion. The experimental result indicated by the black dotted curve shows a large number of peaks that could indicate the existence of background noise, from both the tank and instrumentation, as well as wave reflections from the tank walls. Since this will difficult the process of analyzing the data, the Savitzky-Golay digital filter is applied, once it acts as a low-frequency band pass and smooths the data, indicating the trend of the results (Kennedy, 2020). Two parameters are used to set the options of the filter, the window size, and the polynomial order of the fitting curve. A study of such parameters is performed before hand, so that important data information is not lost.

Despite the existence of peaks that may be associated with background noise, manufacturing imperfections, and reflections due to the tank wall, some of them are related to the natural frequencies of the monopile as they are near the values predicted by the numerical model (indicated by the dashed vertical lines). However, unlike the numerical model, the critical vibration occurs in higher frequency ranges, which can be attributed to the boundary condition at the bottom of the physical monopile, how the load is applied at the top surface, and the monopile is not completely cylindrical. In the further analyses, the ability of reducing vibrations at tailored frequency ranges and consequently the underwater pressure waves of the meta-cushions is investigated.

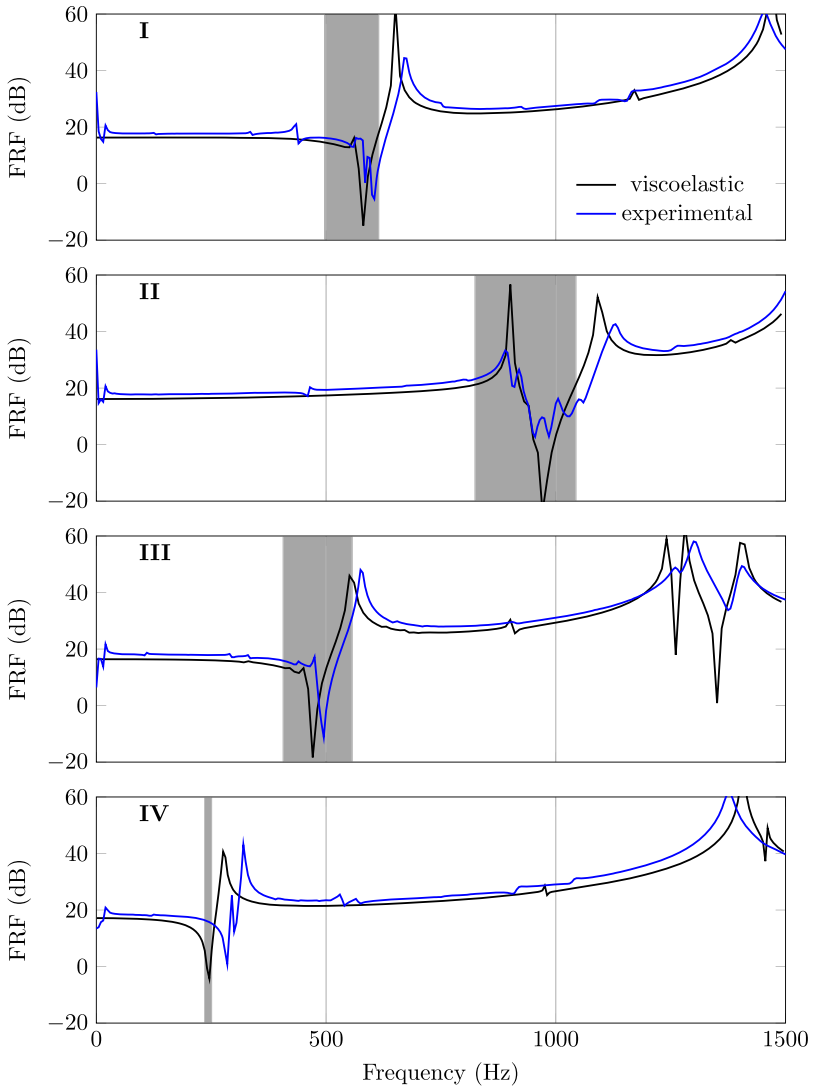

Fig. 11. Comparison between the FRFs obtained through numerical and experimental analyses of spiral arrays. The numerical analysis was performed for both elastic and viscoelastic model of the arrays. The gray areas indicate the band gaps obtained via the dispersion curve analysis.

The transfer functions from the hammering pile containing the single meta-cushions are initially evaluated (cushions A, B, C, and D as indicated in Table 3). To observe the attenuation principle of the meta-cushion, the results are compared with the transfer functions from hammering pile containing a reference cushion formed by six solid arrays.

Fig. 14 shows the acceleration and sound pressure levels measured when hammering the monopile with a cushion A. The gray areas indicate the attenuation frequency zones identified in the experimental analysis of the printed arrays as shown in Fig. 11 and the red dotted curves indicate the response of the reference cushion. Notice that in the pressure sensor response (Fig. 14b), a 6 dB drop is observed at the left edge of the predicted attenuation zone, which also matches the decrease in vibration in the monopile wall (Fig. 14a). Similarly as predicted by the numerical model, the attenuation of cushion A is not significant, while the band gap is narrow, however, it could be improved by increasing the amount of resonators.

Unlike the previous cushion, the measurements of the monopile containing a cushion B show insightful remarks, as indicated in Fig. 15. It may be assumed the attenuation performance of cushion B is not significant when comparing the response with the reference cushion. However, as observed in the case of cushion A, the meta-cushion introduces a natural frequency which also fells at the same region of attenuation of array type II, causing a reduction in FRF. This can be better observed when comparing the frequency responses of cushion A and B, as shown in Fig. 18, where the pressure transfer function drops significantly in the higher edge of the attenuation zone. Similarly to the previous case, the attenuation is more pronounced at the lower edge of the band gap–where a drop of 7 dB is observed–and it decreases along the bandwidth. This highlights the asymmetric feature of local-resonant metamaterials. However, the bandwidth is larger than that of the previous configuration, especially due to the frequency-dependent characteristic of viscoelastic materials. Similar behavior is also observed in the hydrophone measurements, as shown in Fig. 15c.

Fig. 16 shows the measurements for the case of a monopile with a cushion of configuration C. Although a significant reduction of sound levels is not observed in the band gap range, a drop is clearly observed in the vibration of the monopile wall, as indicated in Fig. 16a. However, a clear increase of sound level and monopile vibration at frequencies higher than 900 Hz is observed, which can indicate that this array is not suitable for the noise attenuation in case of monopiles generating critical noise levels at such range. Similar behavior is also observed in the hydrophone measurements, as shown in Fig. 16c.

Fig. 17 shows the measurements for the case of a monopile with a cushion of configuration D. As observed in the numerical evaluation,

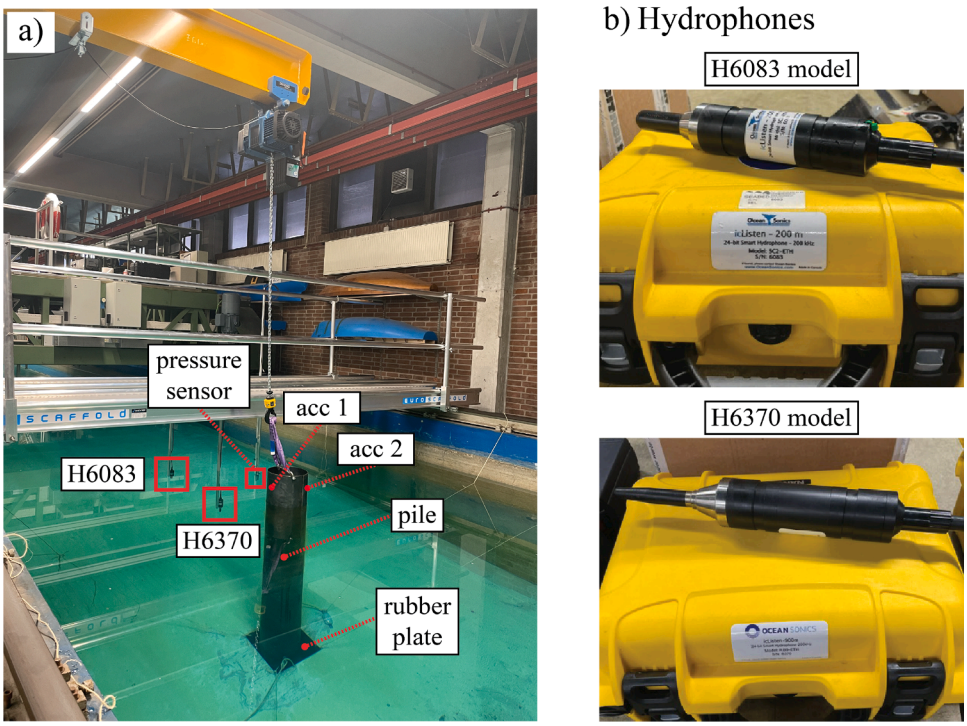

Fig. 12. a) Experimental setup for measurement of noise during pile hammering. The monopile is positioned inside the tank with the aid of a crane and a rubber plate. The accelerometer positions are indicated by acc 1 and acc 2. The hydrophones are aligned with the monopile at a distance of 1 m (H6370) and 2 m (H6083) from the pile. b) Hydrophones 6083 and 6370 used to capture the underwater noise.

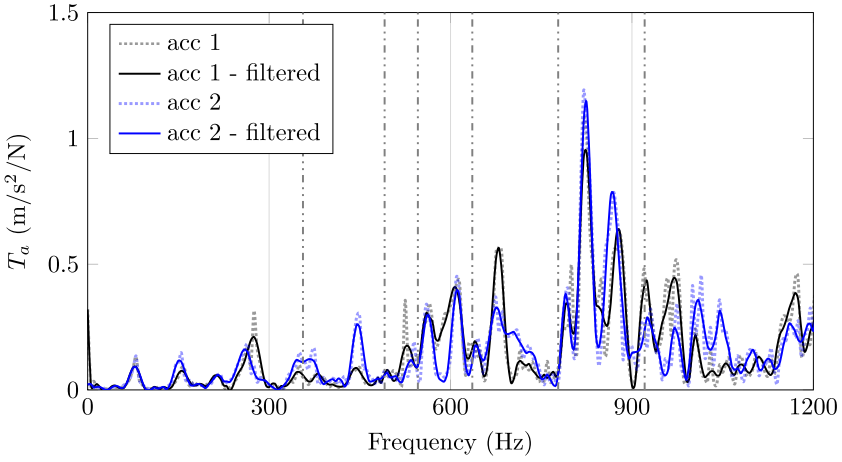

Fig. 13. FRF of radial acceleration of a monopile without cushion for numerical and physical models. The black dashed curve indicates the FRF without filtering. The vertical lines indicate the natural frequencies extracted from the numerical model, also displayed in Fig. 3.

this design does not show significant contributions to attenuate noise. The pile vibration is only reduced at the lower edge of the band gap, which has not been enough to reduce the noise levels, as indicated by the pressure sensor 17b and the hydrophone measurement 17c. However, unlike the previous designs, this cushion has a much lower frequency response function at frequencies higher than 900 Hz.

The noise attenuation performance is also evaluated for meta-cushions with combined configurations, where the results are presented in Figs. 18–21. In Fig. 18, the pressure transfer functions of the single configurations A (array I) and B (array II) are repeated and compared with combined configuration 1 (arrays I and II). Notice that the single cushions exhibit reduced response at their respective band gaps, while the combined cushion demonstrate a certain average of each single cushion contribution. Even though the array I does not show an expressive band gap, it can still be used to attenuate possible natural frequencies of the designed cushion, prohibiting its propagation to the monopile vibration. Similar behavior is observed in Fig. 19, where it can also be highlighted that the high peak induced by cushion C (array III) reduces in about 30 dB when combined with cushion B (array II), as shown by the curve of combined cushion 2 (arrays II and III). Interestingly, the combined configuration 3 has shown the lowest pressure levels at the frequency range around 900 Hz, in comparison to the previous configurations. Because array IV does not induce peaks at this range and since array II induces band gap at this range, the attenuation is amplified, being the lowest drop below 100 dB (see Fig. 20). Finally, Figs. 21 and 22 indicate the pressure levels induced by combined cushions 4 and 5, respectively, where once again reinforce the superposition effect when different resonators are combined. Particularly for combined cushion 5, it can be highlighted that the pressure levels are below 140 dB for the full frequency range under investigation.

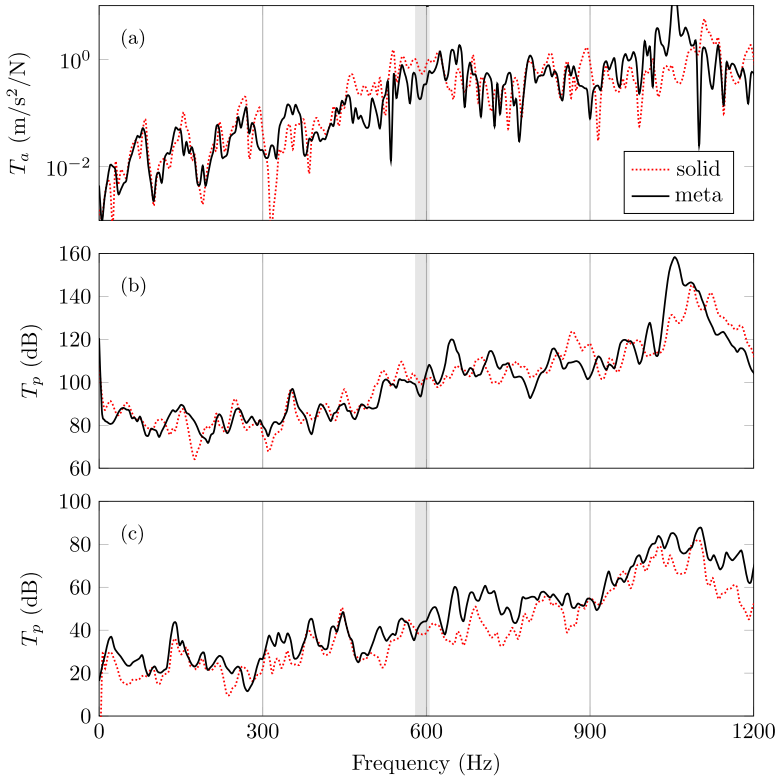

Fig. 14. Comparison between transfer functions obtained by hammering a monopile containing a reference cushion and cushion A. a) Response at pile wall, b) response from pressure sensor c) response from hydrophone sensor.

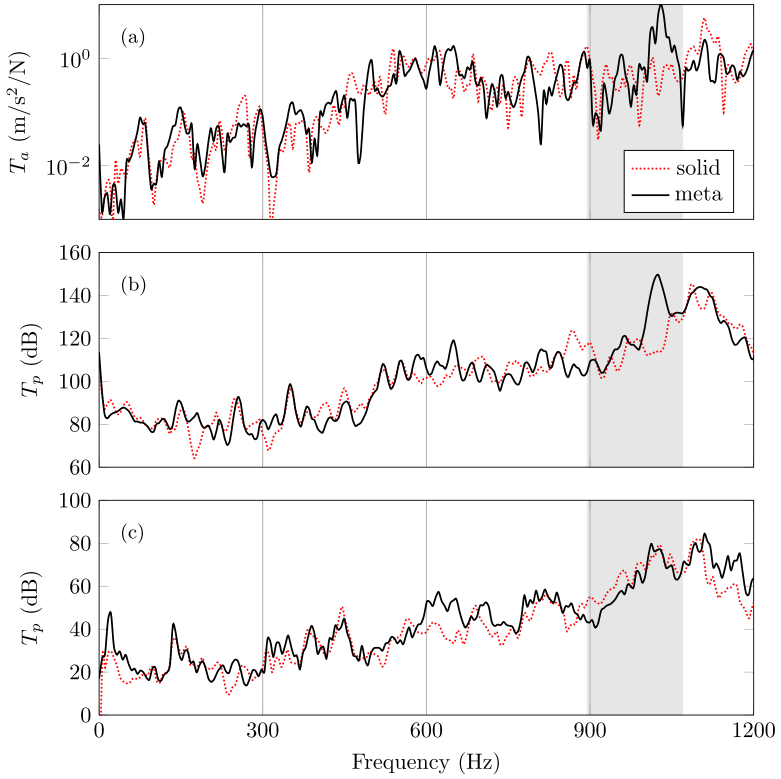

Fig. 15. Measurement from accelerometer and pressure sensors for hammering a monopile containing a cushion B. a) Response at pile wall, b) response at the pressure, and c) response measured by the hydrophone. The band gap of the spiral unit cell is indicated by the gray area.

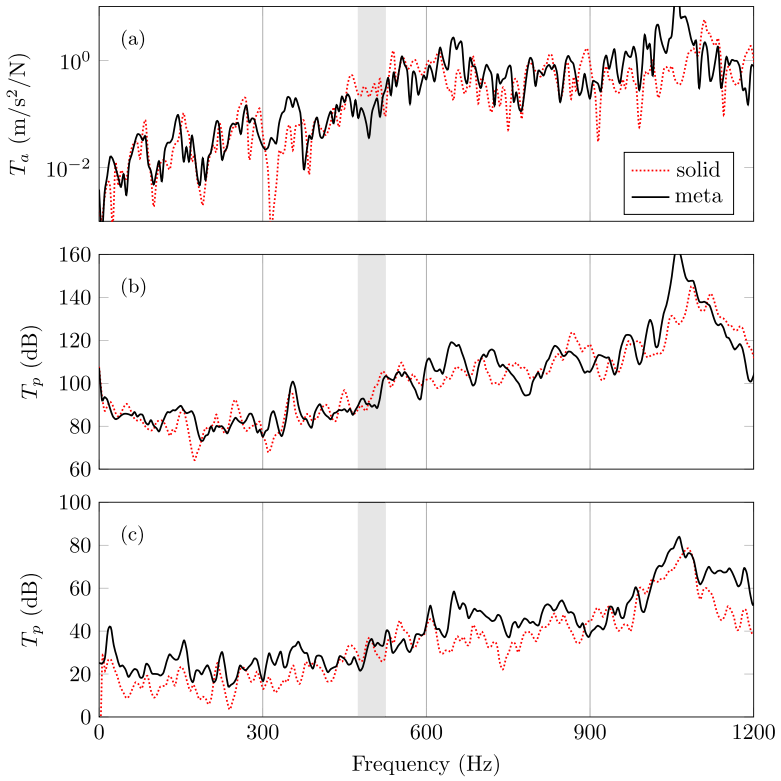

Fig. 16. Measurement from accelerometer and pressure sensors for hammering a monopile containing a cushion C. a) Response at pile wall, b) response at the cushion, and c) response measured by pressure sensor inside the tank. The band gap of the spiral unit cell is indicated by the gray area.

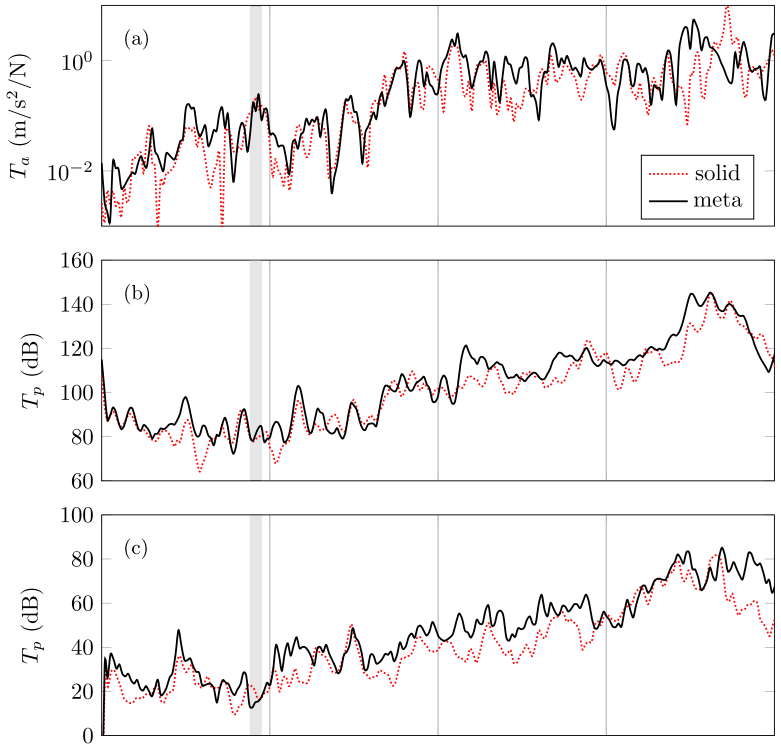

Fig. 17. Measurement from accelerometer and pressure sensors for hammering a monopile containing a cushion D. a) Response at pile wall, b) response at the cushion, and c) response measured by pressure sensor inside the tank.

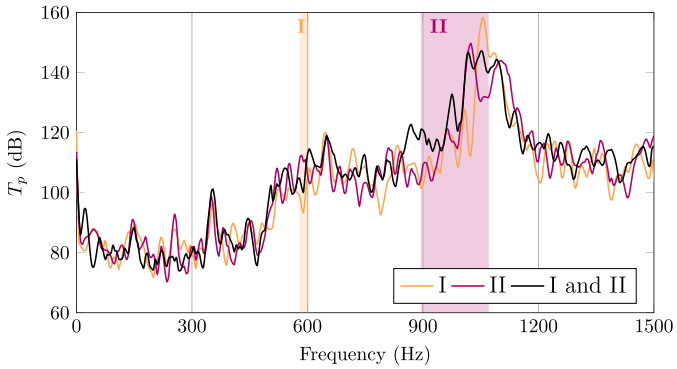

Fig. 18. Comparison of pressure sensor measurements among impact tests with cushion A, B, and comb1 from Table 3. Band gaps have been highlighted according to the resonator type.

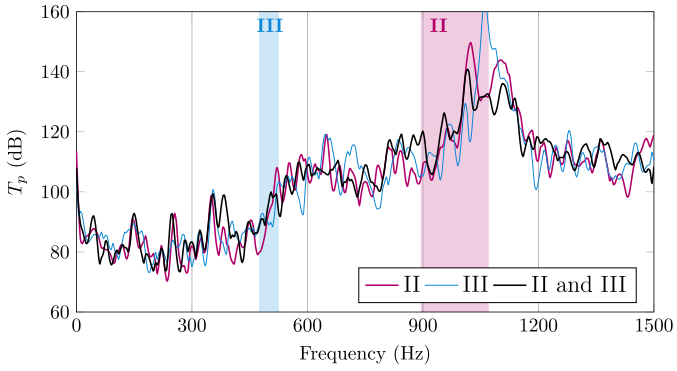

Fig. 19. Comparison of pressure sensor measurements among impact tests with cushion B, C, and comb2 from Table 3. Band gaps have been highlighted according to the resonator type.

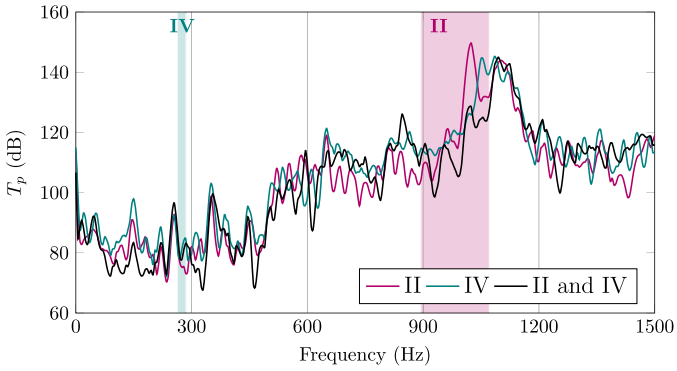

Fig. 20. Comparison of pressure sensor measurements among impact tests with cushion B, D, and comb3 from Table 3. Band gaps have been highlighted according to the resonator type.

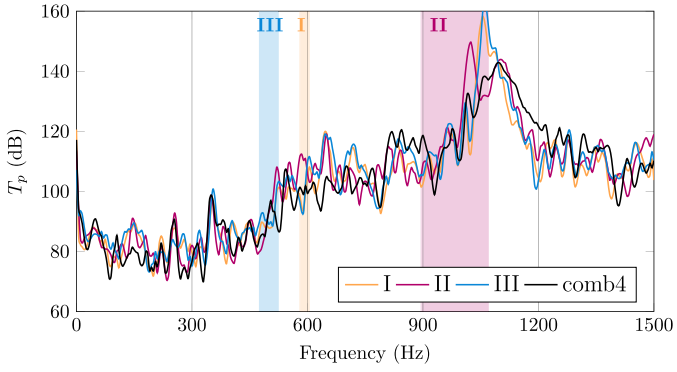

Fig. 21. Comparison of pressure sensor measurements among impact tests with cushion A, B, C, and comb4 from Table 3. Band gaps have been highlighted according to the resonator type.

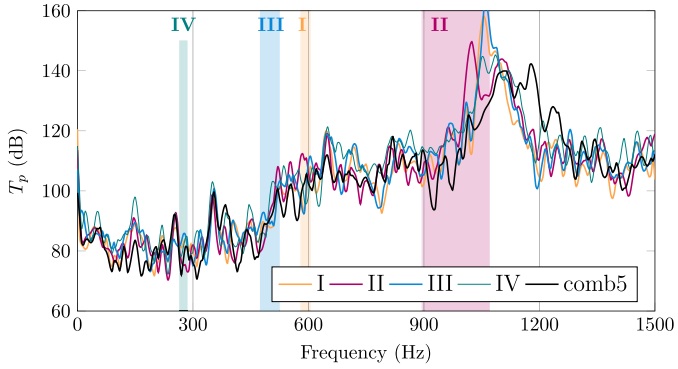

Fig. 22. Comparison of pressure sensor measurements among impact tests with cushion A, B, C, D, and comb5 from Table 3. Band gaps have been highlighted according to the resonator type.

Table 5
SPL reduction observed in the designed band gap of each single meta-cushion configuration.

Band gap	Meta-cushion		SPL eduction
I (580 Hz)	ref: 102 dB	A: 99 dB	3 dB
II (895 Hz)	ref: 117 dB	B: 105 dB	12 dB
III (475 Hz)	ref: 88 dB	C: 90 dB	–2 dB
IV (265 Hz)	ref: 80 dB	D: 80 dB	0 dB

Table 6
SPL observed in the designed band gap of each combined meta-cushion configuration. The SPL indicated in bold represent the designed band gaps of each combined cushion.

Band gap	Meta-cushion				
	comb1	comb2	comb3	comb4	comb5
I (580 Hz)	**104**	109	98	**101**	**97**
II (895 Hz)	**120**	**118**	**112**	**116**	**113**
III (475 Hz)	81	**88**	80	**84**	**82**
IV (265 Hz)	74	74	**84**	74	**77**

An overview of SPL reduction for each meta-cushion configuration is provided in Table 5. The SPL values were selected at the left edge of each designed band gap. For cushions with single resonators, reductions were measured relative to the reference cushion; for combined configurations, comparisons were made among themselves. As indicated in Table 5, meta-cushion B exhibited the highest SPL reduction at its designed band gap, demonstrating a potential design to be explored in full-scale applications. For combined configurations, Table 6 lists SPLs at the lower edge of each band gap, with configuration comb5 generally showing the lowest values.

6. Nondimensional investigation of spiral resonator

As meta-cushions formed by arrays of type II give the best attenuation performance in a wider band gap range, this resonator design has been selected to perform a nondimensional investigation and predict the attenuation zones for different unit cell sizes and materials, constituting then the final block of the design methodology. To that end, nondimensional dispersion curves are extracted by considering an infinite periodic system formed by resonators II. Such problem can be reduced by applying periodic boundary conditions on a single unit cell (Hussein et al., 2014). Fig. 23 shows the dispersion relation curve of the proposed unit cell. The nondimensional frequency is defined as $\Omega = fa/c$, where f is the eigenfrequency obtained for each wave vector $\mathbf{k}$, a is the unit cell size, and c is the wave speed, given as $c = \sqrt{E/\rho}$. Two band gaps are observed between nondimensional frequency ranges [0.0206,0.0263] and [0.0337,0.0363]. By providing either the unit cell size a or material parameters that define the velocity c, the band gap can be adjusted according to required critical noise levels, as shown in Tables 7 and 8. This allows to adapt the meta-cushion design for monopiles from different

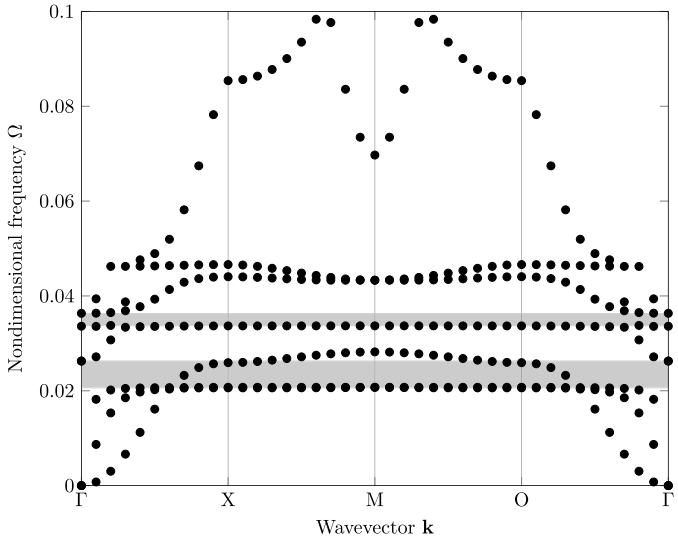

Fig. 23. Nondimensional dispersion curve of spiral resonator type II. The gray area indicates the band gap in the in-plane direction.

Table 7
First band gap range, in Hertz, for unit cells of different sizes and materials.

Material	Unit cell size a			
	0.01 m	0.04 m	0.1 m	0.4 m
PLA	[3275, 4181]	[819, 1045]	[327, 418]	[82, 104]
Aluminium	[10,489, 13,391]	[2622, 3347]	[1048, 1339]	[263, 335]
Steel	[10,781, 13,764]	[2695, 3441]	[1078, 1376]	[269, 344]

Table 8
Second band gap range, in Hertz, for unit cells of different sizes and materials.

Material	Unit cell size a			
	0.01 m	0.04 m	0.1 m	0.4 m
PLA	[5358, 5771]	[1339, 1045]	[536, 577]	[134, 144]
Aluminium	[17,159, 18,483]	[4289, 3347]	[1715, 1848]	[429, 462]
Steel	[17,637, 18,997]	[4409, 3441]	[1763, 1899]	[441, 475]

dimensions or even when such monopiles induce more than one critical noise zone. The different material choices also allow the exploration of meta-cushion designs that undergo from low-energy to high-energy impact hammers.

7. Conclusions

This paper introduces a novel methodology for designing meta-cushions to reduce underwater noise during monopile installations. The methodology is adaptable to any hammering process, as it tailors the cushion design to the specific input parameters of each installation. Numerical and experimental analyses are performed to demonstrate the meta-cushion's ability to attenuate noise while withstanding high hammer-induced stresses. A nondimensional analysis further enables the selection and scaling of optimal designs for full-scale installations.

A case study was used to demonstrate each step of the design methodology, yielding several key findings. The comparison between numerical and experimental results confirmed that the noise attenuation is attributed to the meta-cushion's band gaps, which can occur at single or multiple frequency ranges depending on the resonator configuration. The multi-resonator design, in particular, demonstrated a promising solution in achieving broader attenuation zones, which could be beneficial when multiple frequency zones exhibit critical noise levels. Incorporating viscoelastic properties into the numerical model also improved the accuracy of the predicted band gaps.

While some assumptions regarding material selection and boundary conditions were necessary to demonstrate the design methodology, refining these choices could reduce uncertainties observed in the experiments and anticipated in full-scale analyses. In terms of the meta-cushion, alternative materials may help to better capture viscoelastic behavior or enable high-resolution manufacturing techniques. Moreover, investigating the effect of nonperiodic resonators would be beneficial in case of imperfections resulting from the manufacture process. For the scaled monopile, using a single steel sheet could minimize welding effects, and replacing the modal hammer with a scaled impact hammer would provide the energy needed to excite the monopile modes more realistically. Fixing the meta-cushion to the top of the monopile could also minimize rebound or friction effects, aligning better with the perfect contact assumed in the transfer function approach in the numerical simulations. Finally, testing in larger tanks with a soil layer-or conducting on-site measurements with real-sized hammers-would help predict the wave propagation and reflection as well as allow assessment of soil effects on pile dynamics, which may differ between scaled and full-scale conditions. A soil layer would also improve the physical model's boundary condition at the monopile base, which could be implemented in the numerical models. While this work focused on impact hammer installation, other methods-such as vibratory hammers-would require an investigation of the load characteristics to update the input parameters defining the critical frequency ranges.

Finally, the proposed design methodology is not limited only to the design of meta-cushion, but it could also be implemented as a guideline of other metamaterial-based designs for offshore noise mitigation, such as flexible curtains placed around the monopile.

CRediT authorship contribution statement

Ana Carolina Azevedo Vasconcelos: Writing – original draft, Validation, Methodology, Investigation, Conceptualization; **Christof Van Zijl:** Validation, Investigation; **Dingena Schott:** Writing – review & editing, Supervision, Project administration; **Jovana Jovanova:** Writing – review & editing, Supervision, Funding acquisition, Conceptualization.

Declaration of competing interest

The authors declare that they have no known competing financial interests or personal relationships that could have appeared to influence the work reported in this paper.

Acknowledgment

The authors would like to thank Delft University of Technology for enabling this research as a project awarded by the faculty of Mechanical Engineering.

References

Andersson, M.H., Andersson, B.L., Pihl, J., Persson, L.K.G., Sigray, P., Andersson, S., Wikström, A., Ahlsén, J., Hammar, J., 2017. A framework for regulating underwater noise during pile driving.

ASTM, 2008. Standard test method for high-strain dynamic testing of deep foundations.

Bellmann, M.A., 2014. Overview of existing noise mitigation systems for reducing pile-driving noise. Proceeding auf der Internoise.

Bohne, T., Grießmann, T., Rolfes, R., 2019. Modeling the noise mitigation of a bubble curtain. J. Acoust. Soc. Am. 146 (4), 2212–2223.

Bruns, B., Kuhn, C., Stein, P., Gatermann, J., Elmer, K.-H., 2014. The new noise mitigation system' hydro sound dampers': history of development with several hydro sound and vibration measurements. In: INTER-NOISE and NOISE-CON Congress and Conference Proceedings. Vol. 249. Institute of Noise Control Engineering, pp. 4915–4923.

Dahl, P.H., de Jong, C. A.F., Popper, A.N., 2015. The underwater sound field from impact pile driving and its potential effects on marine life. Acoust. Today 11 (2), 18–25.

Deeks, A.J., Randolph, M.F., 1993. Analytical modelling of hammer impact for pile driving. Int. J. Numer. Anal. Methods Geomech. 17 (5), 279–302.

Deng, Q., Jiang, W., Zhang, W., 2016. Theoretical investigation of the effects of the cushion on reducing underwater noise from offshore pile driving. J. Acoust. Soc. Am. 140 (4), 2780–2793.

Hussein, M.I., Leamy, M.J., Ruzzene, M., 2014. Dynamics of phononic materials and structures: historical origins, recent progress, and future outlook. Appl. Mech. Rev. 66 (4), 1–38.

Kastelein, R.A., Gransier, R., Marijt, M.A.T., Hoek, L., 2015. Hearing frequency thresholds of harbor porpoises (Phocoena phocoena) temporarily affected by played back offshore pile driving sounds. J. Acoust. Soc. Am. 137 (2), 556–564.

Kennedy, H.L., 2020. Improving the frequency response of savitzky-golay filters via colored-noise models. Digit. Signal Process. 102, 102743.

Kontou, E., Charitos, I., Drougkas, A., 2024. Modeling the fundamental viscoelastic properties of polylactic acid (PLA) and PLA/nanocomposites in a unified manner. Nanomaterials 14 (13), 1116.

Lee, K.M., Wochner, M.S., Wilson, P.S., 2012. Mitigation of low-frequency underwater anthropogenic noise using stationary encapsulated gas bubbles. In: Proceedings of Meetings on Acoustics. Vol. 17. AIP Publishing.

Leng, J., Lan, X., Liu, Y., Du, S., 2011. Shape-memory polymers and their composites: stimulus methods and applications. Prog. Mater. Sci. 56 (7), 1077–1135.

Ma, Y., Yang, J., 2023. Earth pressure distribution on laterally loaded offshore monopiles. Ocean Eng. 273, 113954.

Murphy, G., Igoe, D., Doherty, P., Gavin, K., 2018. 3d FEM approach for laterally loaded monopile design. Comput. Geotech. 100, 76–83.

Muthui, Z.W., Kamweru, P.K., Nderitu, F.G., Hussein, S.A., Ngumbu, R., Njoroge, G.N., 2015. Polylactic acid (PLA) viscoelastic properties and their degradation compared with those of polyethylene. Int. J. Phys. Sci. 10, 568–575.

von Pein, J., Lippert, T., Lippert, S., von Estorff, O., 2022. Scaling laws for unmitigated pile driving: dependence of underwater noise on strike energy, pile diameter, ram weight, and water depth. Appl. Acoust. 198, 108986.

Reinhall, P.G., Dahl, P.H., 2011. Underwater mach wave radiation from impact pile driving: theory and observation. J. Acoust. Soc. Am. 130 (3), 1209–1216.

Solé, M., Sigray, P., Lenoir, M., van der Schaar, M., Lalander, E., André, M., 2017. Offshore exposure experiments on cuttlefish indicate received sound pressure and particle motion levels associated with acoustic trauma. Sci. Rep. 7 (1), 1–13.

Thumsorn, S., Prasong, W., Kurose, T., Ishigami, A., Kobayashi, Y., Ito, H., 2022. Rheological behavior and dynamic mechanical properties for interpretation of layer adhesion in FDM 3d printing. Polymers 14 (13), 2721.

Tsouvalas, A., 2020. Underwater noise emission due to offshore pile installation: a review. Energies 13 (12), 3037.

Vasconcelos, A.C.A., Valappil, S.V., Schott, D., Jovanova, J., Aragón, A.M., 2024. A metamaterial-based interface for the structural resonance shielding of impact-driven offshore monopiles. Eng. Struct. 300, 117261.

Wang, H., Wang, L.Z., Hong, Y., He, B., Zhu, R.H., 2020. Quantifying the influence of pile diameter on the load transfer curves of laterally loaded monopile in sand. Appl. Ocean Res. 101, 102196.

Wind Europe. Wind energy in Europe: 2021 statistics and the outlook for 2022–2026. 2022.